Volume 14, Number 4, 2021. pp. 287-299

Jordan Journal of Physics

ARTICLE

Investigation of the Structural and Magnetic Properties of BaM Hexaferrites Prepared from Scrap Iron Filings

Eman S. Al-Hwaitat[a], **Mohammad K. Dmour**[a], **Ibrahim Bsoul**[b], **Abeer Albgour**[a], **Tuqa Alsalti**[a], **Raghad Abuawad**[a], **Aseel Alajarmah**[a], **Rola Al-Buqain**[c] and **Sami H. Mahmood**[a,d]

[a] *Physics Department, The University of Jordan, Amman 11942, Jordan.*
[b] *Physics Department, Al al-Bayt University, Al-Mafraq 13040, Jordan.*
[a] *The Cell Therapy Center, The University of Jordan, Amman 11942, Jordan.*
[b] *Department of Physics and Astronomy, Michigan State University, East Lansing, MI 48824, USA.*

Doi: **https://doi.org/10.47011/14.4.2**

Received on: 07/05/2020; *Accepted on: 12/11/2020*

Abstract: In this work, we demonstrate the feasibility of preparing a commercially important type of magnetic oxide, BaM ($BaFe_{12}O_{19}$) hexaferrite, using scrap iron filings as an iron source. The hexaferrites were prepared by conventional solid state reaction and characterized by X-ray diffraction (XRD), scanning electron microscopy (SEM) and magnetization measurements. XRD patterns of samples prepared by mixing powders extracted from the iron filings with appropriate amounts of barium carbonate and sintering at 1200 °C revealed the presence of a major BaM hexaferrite with small amounts of nonmagnetic α-Fe_2O_3 oxide phase. On the other hand, SEM images of the samples showed clear crystallization of perfect hexagonal platelets of BaM hexaferrite, which was further confirmed by the Curie temperature determined from the thermomagnetic measurements. The saturation magnetization of the samples was in the range of 45.1– 52.1 emu/g and the remnant magnetization in the range of 14.8 – 19.0 emu/g. These values and the moderate coercivity of ~ 1 kOe suggest that the prepared samples could potentially be useful for high-density magnetic recording.

Keywords: Hexaferrite, Solid waste, Magnetic Properties, Structural properties, Magnetic recording.

Introduction

The revolutionary growth in modern industrialization, mining and technological advances did not proceed without leaving behind negative impacts on the environment, partially caused by the accumulation of hazardous solid wastes [1-4]. For example, the industry connected to canned food, steel and iron production plants, disposable parts of vehicles and utilities and by-products of machining contribute significantly to the increasing level of such solid waste on planet Earth. Wise planning for avoiding this problem should not be limited to wise disposal of such waste, but should also benefit from the feasibility of recycling solid wastes in the production lines. This process would provide alternative sources of materials necessary for the industry, thus reducing both the demand for mining in search of naturally occurring minerals and the level of solid waste.

For decades, magnetic oxides have been widely used in a wide range of applications in our everyday life [5-9], thus contributing significantly to efficient achievement of tasks and convenience in human societies. The

Corresponding Author: Sami H. Mahmood **Email**: s.mahmood@ju.edu.jo

competitiveness of magnetic oxides in the industrial market was not established by their performance only, but also by their cost effectiveness. The cost of production of materials for applications is determined by several parameters, including the cost of raw materials and processing. Thus, adopting successful strategies for cost-effective use of recyclable materials provides additional benefits in producing high-performance materials, while conserving natural resources and significantly reducing cost. Specifically, magnetic oxides could be produced from recycled iron-rich scrap, thus cutting down the cost of raw materials. The aim of this article is to demonstrate an effective procedure for the use of scrap iron in the production of beneficial materials for permanent magnet applications. While this procedure is concerned with the use of a specific iron scrap (iron filings resulting from machining processes), the procedure could be extended to other iron scrap sources, including iron-rich food cans, metal parts and byproducts of mining and industrialization.

M-type hexagonal ferrite ($MFe_{12}O_{19}$, where M = Ba, Sr, Pb) is an important functional magnetic oxide possessing high magnetocrystalline anisotropy and relatively high saturation and remanence magnetization. The large annual production of these materials was motivated by their cost-effectiveness and suitability for a wide range of applications [5-8, 10-14]. Consequently, the production of these ferrites and investigation of their structural and physical properties have received an exponentially increasing interest in the last few decades [15-21]. In this article, we describe the preparation of M-type barium hexaferrite using iron-rich scrap metal filings without the need for prior knowledge of the exact elemental contents of this iron source. The large-scale employment of this procedure is promising for providing important magnetic materials at low cost and efficient disposal of solid wastes.

Experimental Work

Preparation of the Starting Iron-rich (F) Powder

Scrap iron filings resulting from machining iron rods and objects in the mechanical workshop at the Physics Department, the University of Jordan, were collected using a bar magnet to avoid nonmagnetic particles in the collected raw material. The collected filings are expected to consist of mainly metallic iron, but may also contain small amounts of other elements due to impurities in the machined iron objects and contamination due to possible mixing with small amounts of particles of other materials such as Al and brass, which are normally processed by the same device. The filings were washed with water and preheated at 500 ºC for 2 h to get rid of moisture, oils and other non-metallic burnable materials. The preheated material was subsequently hand-ground in an agate mortar and pestle for 1 h. The resulting powder (labelled F) was strongly attracted to a small magnet, indicating that the above heat treatment did not result in appreciable conversion of metallic iron into a non-magnetic (α-Fe_2O_3) oxide phase. This (F) powder was used as a starting iron source for the preparation of BaM hexaferrites.

Preparation of BaM Samples

BaM hexaferrites ($BaFe_{12}O_{19}$) were prepared by conventional solid state reaction using precursor powder mixtures of the F powder and $BaCO_3$ (Sigma-Aldrich made, ~ 99% pure). The production of BaM hexaferrite with high purity can be achieved by sintering a precursor mixture with F/$BaCO_3$ mass ratio (R) consistent with the Fe:Ba stoichiometric molar ratio of 12:1 in BaM. If the F powder consists of pure metallic iron, the stoichiometric composition of BaM requires F/$BaCO_3$ mass ratio of R = 3.40 ($= 12 \times M(\mathrm{Fe})/M(\mathrm{BaCO_3})$, where M is the molar mass). However, if the F powder consists of iron oxide (Fe_2O_3), the required F/$BaCO_3$ mass ratio should be R = 4.85 ($= 6 \times M(\mathrm{Fe_2O_3})\ /\ M(\mathrm{BaCO_3})$. Accordingly, in the absence of prior knowledge of the exact nature (level of oxidation) and composition of the F powder, three powder mixtures with F/$BaCO_3$ mass ratios of R = 3.0 (BFO3), R = 3.5 (BFO3.5) and R = 5.0 (BFO5) were prepared to cover the range between the value corresponding to pure metallic iron and that corresponding to fully oxidized iron. The ratios of R = 3.0 and 3.5 were chosen around the stoichiometric ratio corresponding to pure iron, where slightly lower and higher values were adopted to account for possible presence of small amounts of elements with lower or higher molar masses compared to iron, small amounts of non-reacting impurities or low-levels of oxidation in the F powder. However, the mixture with R = 5.0 was made slightly higher than the stoichiometric mass ratio for Fe_2O_3 to account for possible presence of small amounts of non-reacting impurities in a fully oxidized iron powder. These powder mixtures were hand-ground in an agate mortar and pestle for 1 h and disk-like pellets (1.25 cm in diameter and ~ 2 mm thick) were prepared from the finely ground powder mixtures using a force of 50 kN. The disks were then sintered in air at 1200º C for 2 h, using a heating rate of 10 °C/min. For the sake of comparison, a pellet of the F powder (without the addition of $BaCO_3$) was prepared and sintered in air at 1200º C for 2 h (resulting in the sample labelled FO). All sintered samples were then characterized structurally and magnetically to investigate the structural phases in the samples and draw conclusions regarding the nature of the filings used as an iron source and the purity of BaM phase in the prepared hexaferrite samples.

The results of the characterization revealed that the FO sample consists of high-purity α-Fe_2O_3 phase (as discussed in a forthcoming subsection). Accordingly, the FO powder was used as a known iron source to prepare a forth BaM sample using a mixture with FO/$BaCO_3$ mass ratio of R = 4.8 (sample BFO4.8), slightly lower than the theoretical ratio (R = 4.85) to account for possible existence of traces of un-oxidized iron at the core of the particles. This powder mixture was pelletized following the abovementioned procedure for the F/$BaCO_3$ mixtures and similarly sintered at 1200 °C for 2 h.

Characterization Techniques

The XRD patterns of the samples were recorded at room temperature using XRD 7000-Shimadzu diffractometer with Cu-K_α radiation (λ = 1.5406 Å). The structural phases in the samples were identified by analyzing the XRD patterns using X'pert HighScore software, whereas the refined structural parameters were obtained by Rietveld analysis [22] using FullProf software [23, 24]. The XRD patterns were collected in the angular range $20° \leq 2\theta \leq 70°$ in steps of 0.01° and using a scanning speed of 0.5°/min. Scanning electron microscopy (SEM) using Versa 3D, FEI electron microscope was employed to further characterize the samples by examining the morphology and particle size distribution. The magnetic properties of the samples were investigated by room-temperature hysteresis loop measurements using a conventional vibrating sample magnetometry (VSM MicroMag 3900, Princeton Measurements Corporation) operating under an applied magnetic field up to ± 10 kOe. To further confirm the identity of the magnetic phases in the samples, thermomagnetic measurements were performed by measuring the temperature-dependent magnetization under an applied field of 100 Oe in a temperature range up to 550 °C.

Results and Discussion

Characterization of the FO Powder

The sintered FO sample was characterized by XRD, SEM and magnetic measurements. Fig. 1a revealed that the diffraction pattern of the FO powder matches the standard pattern (01-086-2368) for α-Fe_2O_3 oxide phase, confirming the oxidation of the sintered filings. The SEM image in Fig. 1b revealed the presence of rhombohedral, sharp-edged particles with typical size in the range of 1 – 4 µm. These particles are characteristic of α-Fe_2O_3 iron oxide as confirmed by Energy Dispersive X-ray spectroscopic analysis in a previous study [25]. However, the magnetic hysteresis loop in Fig. 1c indicated the presence of a soft magnetic component, which may be associated with small amounts of un-oxidized iron. The saturation magnetization (σ_s) of the sintered powder is ~ 6 emu/g, which is ~ 3% of the saturation magnetization for metallic iron (σ_s = 197 emu/g) [5]. This is an indication that the wt.% of un-oxidized iron in the FO powder is a few percent and the likelihood that this magnetic phase is at the core of the powder particles made it undetectable by XRD measurements. Similarly, in a recent article [26], the ferromagnetic-like behaviour of α-Fe_2O_3 was attributed to Fe-containing impurity with relatively high saturation magnetization. However, in an earlier study, this behaviour was associated with magnetic disorder in the shell of the hematite nanoparticles [27].

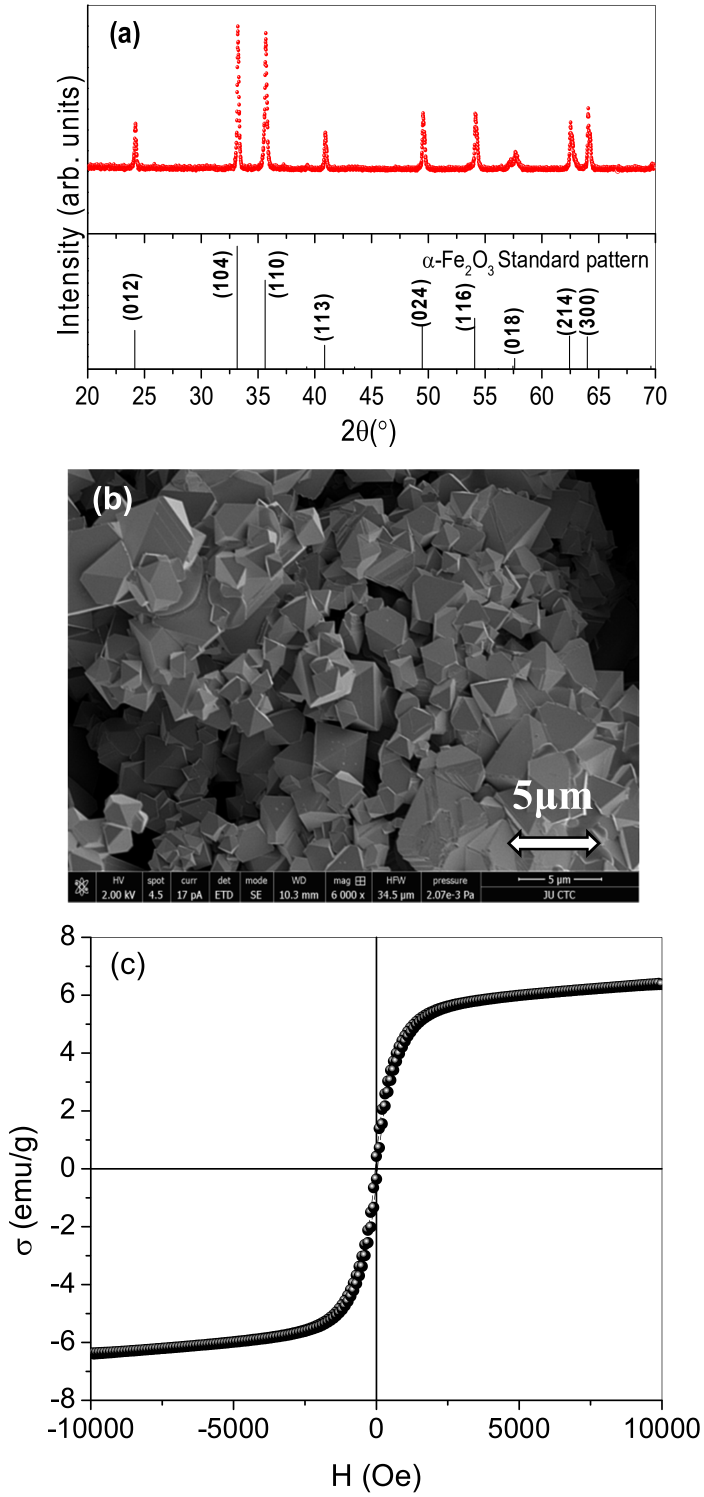

FIG. 1. (a) XRD pattern, (b) SEM image and (c) magnetization curve of the FO sample.

Structural analysis of BaM samples

The three M-type hexaferrites prepared from the F powder (BFO3, BFO3.5, and BFO5) and the forth prepared from the FO powder (BFO4.8) were examined by XRD to investigate the phase purity and the structural characteristics of the hexaferrite phase in these samples. Fig. 2 shows XRD patterns with Rietveld refinement for the BFO3 and BFO3.5 samples. The patterns revealed structural peaks corresponding to a major BaM phase matching the standard pattern (00-043-0002) and a minor nonmagnetic α-Fe_2O_3 oxide phase matching the standard pattern (01-086-2368). The expanded pattern in Fig. 3a indicated that the BFO3 sample contained additional traces of $BaFe_2O_4$ phase as indicated by the weak peak labeled by (B) and of an unidentified phase represented by the weak peak labeled by (⁑). These trace phases were not observed in the pattern of the sample BFO3.5 (Fig. 3b), indicating that these phases most probably contain Ba, which was incorporated in the production of the hexaferrite phase in this sample. The diffraction peaks of the M-type phase are slightly shifted to higher angles by ~ 0.05° compared with the Bragg positions of the standard pattern (Fig. 3), indicating a slight decrease of the lattice constants. Also, the relative intensities of the (006) and (008) Bragg peaks in the pattern of the sample BFO3 (Fig. 2) are obviously higher than in the standard pattern, indicating structural texture along the *c*-axis [28]. In addition, the higher intensities of the peaks corresponding to α-Fe_2O_3 phase in the pattern of the sample BFO3.5 indicated a surplus of Fe in this sample, which forms an extra amount of the Fe_2O_3 oxide phase. The weight ratios of the BaM and α-Fe_2O_3 oxide phase in these samples were determined by Rietveld analysis and are listed in Table 1. The relatively low values of the reliability factors (R_B and R_F) and goodness of fit (χ^2) indicate a reliable fit as demonstrated by the (almost) horizontal difference curve (blue line in Fig. 2). The results indicated that the BaM hexaferrite is a major phase in these samples, with 91.7 wt.% in sample BFO3 and 86.3% in sample BFO3.5. The wt.% of the α-Fe_2O_3 phase of 8.3% and 13.7% in these samples, respectively, is in agreement with the detailed structural analysis of the BaM/Fe_2O_3 composites [29]. These results demonstrated that the required mass ratio of the F powder to produce a high purity BaM hexaferrite is lower than the stoichiometric ratio of R = 3.40 for pure iron, which leads to two conclusions regarding the iron filings used in this study. First, the filings in the F powder were mostly in the form of metallic iron, since progressive oxidation should increase the required F/$BaCO_3$ mass ratio up to 4.85 for full oxidation. Second, the filings contain impurity elements having lower atomic masses compared to iron, since the required R is lower than the stoichiometric ratio for pure metallic iron. Notably, when these elements occupy the Fe^{3+} sites in the hexaferrite lattice, they may lead to modifications of the magnetic properties of the hexaferrites.

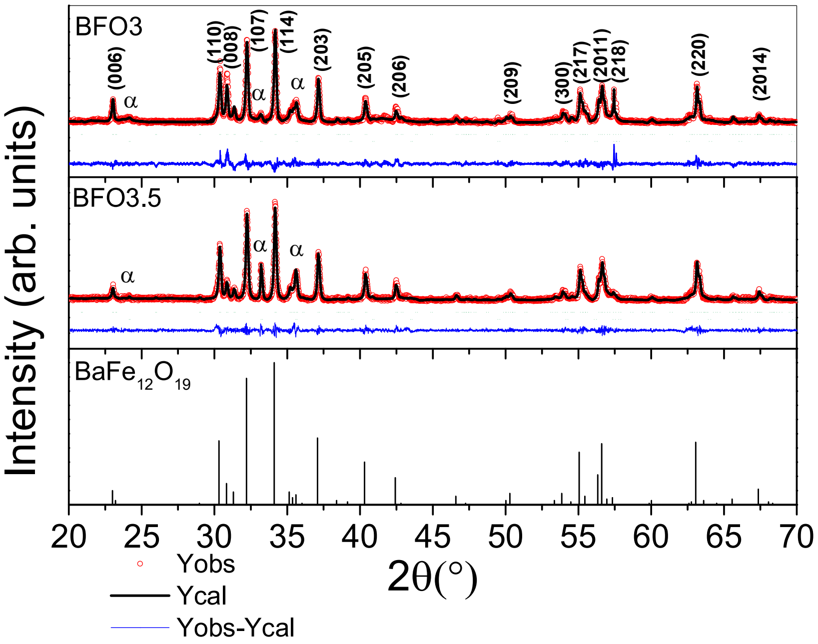

FIG. 2. XRD patterns with Rietveld refinement for sintered BFO3 and BFO3.5 samples. The red open circles represent the experimental data, the black line represents the calculated pattern and the blue line below the pattern represents the difference between the experimental and calculated patterns. The reflections corresponding to α-Fe_2O_3 oxide phase are labeled (α). The standard patterns of M-type hexaferrite is shown for comparison.

(a) BFO3

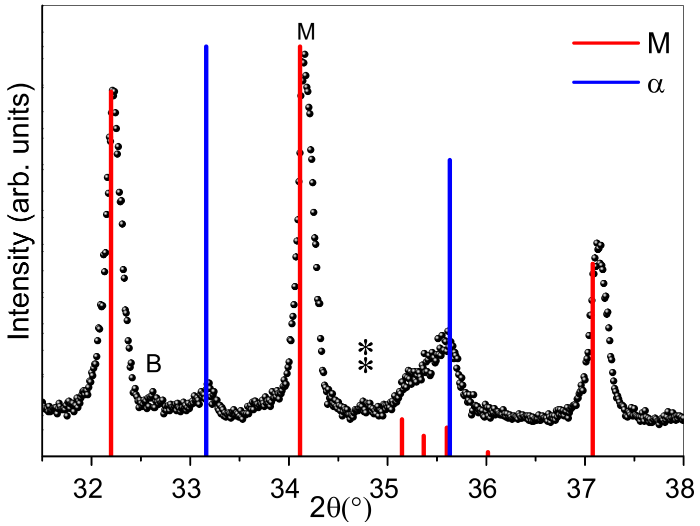

(b) BFO3.5

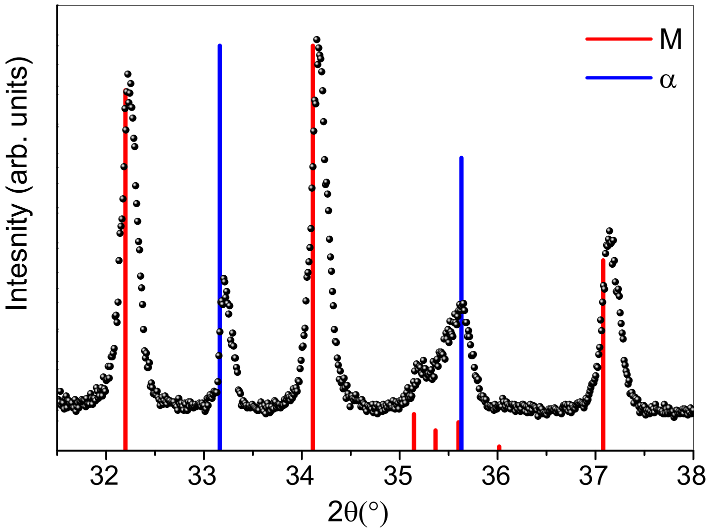

FIG. 3. Expanded view of the diffraction patterns for the samples with F/$BaCO_3$ mass ratio of (a) 3.0:1.0 and (b) 3.5:1.0. The red bars represent the structural peaks in the standard pattern of the M-type, whereas the blue bars are the structural peaks in the standard pattern of α-Fe_2O_3 phase. The peak labeled B corresponds to $BaFe_2O_4$ phase.

TABLE 1. The fractions of the phases (in wt.%) as obtained by Rietveld analysis. The reliability factors and goodness of fit (R_B, R_F, and χ^2) are also listed.

Sample	Phase	Wt.%	R_B	R_F	χ^2
BFO3	BaM	91.7	6.84	5.33	0.61
	α-Fe_2O_3	8.3	6.60	6.21	
BFO3.5	BaM	86.3	3.55	4.12	0.40
	α-Fe_2O_3	13.7	5.56	4.32	
BFO5	BaM	84.1	5.20	5.02	0.69
	α-Fe_2O_3	15.9	6.53	4.92	
BFO4.8	BaM	98.7	4.10	4.87	0.47
	α-Fe_2O_3	1.3	9.83	8.10	

On the other hand, Fig. 4 shows XRD patterns of the samples BFO5 (prepared from the F powder) and BFO4.8 (prepared from the FO powder) with mass ratio close to the stoichiometric ratio for α-Fe_2O_3. The diffraction pattern of sample BFO5 in Fig. 4 (a) revealed the presence of a significant amount of α-Fe_2O_3 phase compared with sample BFO3. The wt.% of iron oxide phase in the sample was determined by Rietveld analysis and found to be 15.9% (Table 1). This is an indication that the F/$BaCO_3$ mass ratio in this sample is significantly higher than the stoichiometric ratio in BaM, confirming the above results which revealed that the F powder is mostly metallic iron, rather than iron oxide. However, Rietveld analysis revealed that the sample BFO4.8 prepared from the pre-oxidized (FO) powder is almost a pure BaM phase (98.7%), confirming that this starting powder consists of α-Fe_2O_3, in agreement with the structural analysis of this powder. The expanded view (Fig. 5) shows that the sample consists of almost a pure M-type phase, with very small amounts of iron oxide impurity phase revealed by the very weak peak at 2θ ~ 33.2° corresponding to the main structural peak of α-Fe_2O_3 phase.

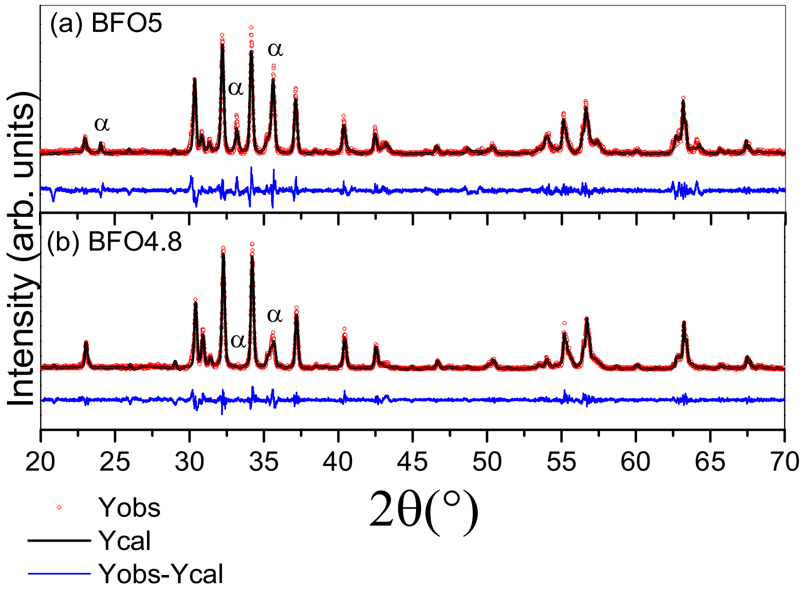

FIG. 4. XRD patterns with Rietveld refinement for the samples BFO5 and BFO4.8.

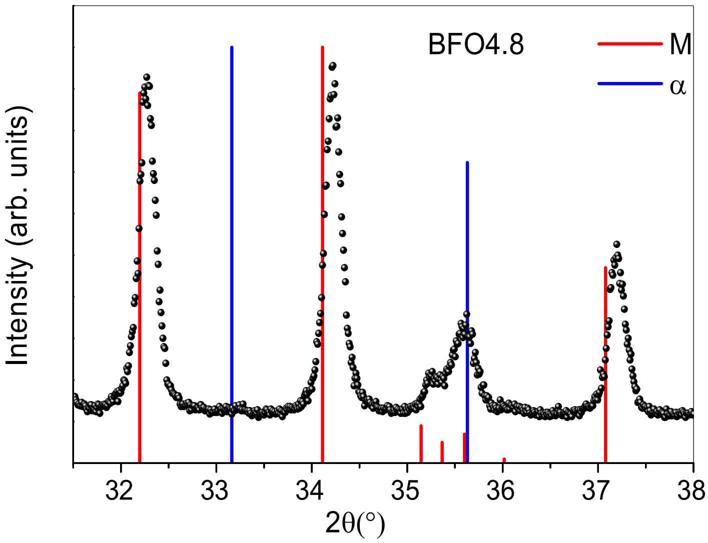

FIG. 5. Expanded view of the diffraction pattern of the sample BFO4.8 in the angular range of the main structural peaks of BaM and α-Fe_2O_3 phases. The Bragg positions and relative intensities of the standard patterns of BaM and α-Fe_2O_3 phases are shown for comparison.

The refined lattice parameters of a = 5.88 – 5.89 Å and c = 23.18 – 23.19 Å for BFO3, BFO3.5 and BFO5 (Table 2) are in good agreement with the standard values of a = 5.89 Å and c = 23.18 Å [30] and the previously reported values of a = 5.897 – 5.899 Å and c = 23.175 – 23.179 Å) [31], but the lattice parameter c is slightly smaller than values in the range of 23.20 – 23.24 Å reported by others [32-34]. However, the lattice parameters of a = 5.88 Å and c = 23.16 Å for BFO4.8 are slightly lower as revealed by the peak shifts in Fig. 5.

TABLE 2. Lattice parameters, cell volume, bulk density, x-ray density and porosity for the samples.

Sample	a (Å)	c (Å)	V (Å^3)	ρ_x (g/cm^3)	ρ_b (g/cm^3)	P%
BFO3	5.89	23.19	696.7	5.30	3.20	40
BFO3.5	5.88	23.18	694.1	5.32	4.13	22
BFO4.8	5.88	23.16	693.5	5.32	4.69	12
BFO5	5.89	23.19	696.7	5.30	4.03	24

The x-ray density was calculated from the molecular weight (M_w) of BaM and the refined cell volume V (Table 2) using the formula:

$$\rho_x = \frac{Z(M_w)}{N_A V} \tag{1}$$

Here, $Z = 2$ is the number of molecules per unit cell and N_A is Avogadro's number. The x-ray density of 5.30 g/cm^3 for BaM phase in BFO3 and BFO5 samples was in agreement with the reported values of 5.28 – 5.29 g/cm^3 [32, 34]. However, the x-ray density of 5.32 g/cm^3 for BaM phase in BFO3.5 and BFO4.8 samples was slightly higher, which is consistent with the slightly lower cell volume in these samples. The bulk density (ρ_b) was measured by Archimedes method and the porosity was calculated using the formula:

$$P\% = \left(1 - \frac{\rho_b}{\rho_x}\right) \times 100 \ . \tag{2}$$

The results in Table 2 indicate that the porosity of the sample BFO3 is significantly higher than in the other samples. However, the range of the observed porosity is slightly lower than the range of 25.8 – 48.4% reported for Mg-Ti substituted BaM [35].

In order to calculate the crystallite size of the BaM phase along the direction perpendicular to the (*hkl*) plane using Stokes and Wilson approach, the corresponding diffraction peak area (A) and maximum peak intensity (I_0) were determined by fitting the peak with a Lorentzian line shape. The integral breadth ($\beta = A/I_0$) was then calculated and the corrected breadth (β_c) was determined by subtracting the instrumental broadening obtained by using a standard Si sample [32]. According to the formulation of Stokes and Wilson, the crystallite size (D) is given by [36]:

$$D = \frac{\lambda}{\beta_c \cos\theta} \tag{3}$$

Here, $\lambda = 0.15406$ nm and θ is the Bragg angle of diffraction peak.

The crystallite size of the BaM phase was determined from its three main reflections (110), (107) and (114) and the results are listed in Table 3. Clearly, the crystallite size along the hexagonal plane (perpendicular to the (110) planes) was not larger than that along the other directions, indicating that the crystallites are not platelet-like in shape.

TABLE 3. Crystallite size of BaM phase along different crystallographic directions.

Sample	Crystallite size*(D)* nm		
	(110)	(107)	(114)
BFO3	151	134	169
BFO3.5	101	141	153
BFO4.8	114	111	115
BFO5	57	98	111

SEM Results

SEM images of the samples revealed the presence of platelet-like particles, some of which exhibiting clear hexagonal symmetry as indicated by the representative images in Fig. 6. Typical particle size in the range of 0.5 – 3.0 μm was observed in all samples except BFO3, which revealed the presence of larger particles with some ~ 10 μm in diameter. In addition, the platelet-like particles are generally thick, the thickness reaching about half the in-plane dimension in some cases. Compared with the crystallite size obtained from analysis of the XRD peaks, the physical particle size is significantly larger, indicating that these particles are polycrystalline.

Magnetic Measurements

The hysteresis loops for the samples are shown in Fig. 7, together with the central part of the loops for clarity. The hysteresis loops revealed that all samples are magnetically semi-hard, with monotonically increasing magnetization in the high-field range, indicating high magnetocrystalline anisotropy field (H_a) in all samples. The coercivity of all samples was in the range of 878 – 966 Oe (Table 4), which is significantly lower than values of 4 – 5 kOe reported for single-domain BaM hexaferrites [37, 38]. However, our observed values are in agreement with values of 860 and 1005 Oe reported by others for samples consisting of large particles as a consequence of the high-temperature sintering at 1300 °C [35, 39]. The reduction of the coercivity in our samples could therefore be due to the multi-domain nature of their constituent particles, in agreement with the SEM images which revealed the presence of a large fraction of particles with size greater than the single-domain critical size of ~ 0.5 – 1 μm [6, 40]. The remanence magnetization (σ_r) was also determined from the hysteresis loops and the results are listed in Table 4. These materials with σ_r in the range of 14.8 – 19.0 emu/g and intermediate values of the coercivity could be used for the production of cost-effective low-performance permanent magnets for applications that do not require high flux and magnetic hardness. However, these characteristics are better suited for high-density magnetic recording applications [21, 41].

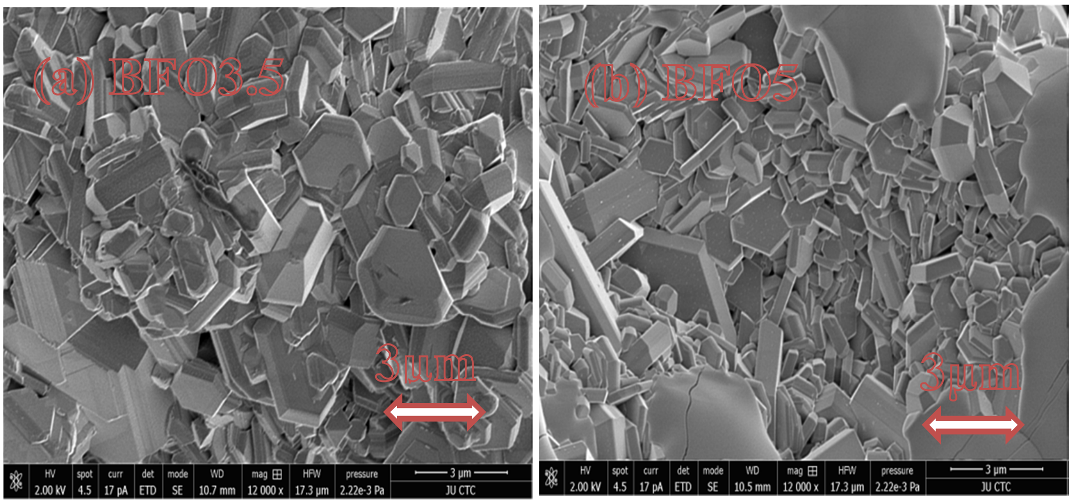

FIG. 6. Representative SEM images for BFO3.5 and BFO5 samples.

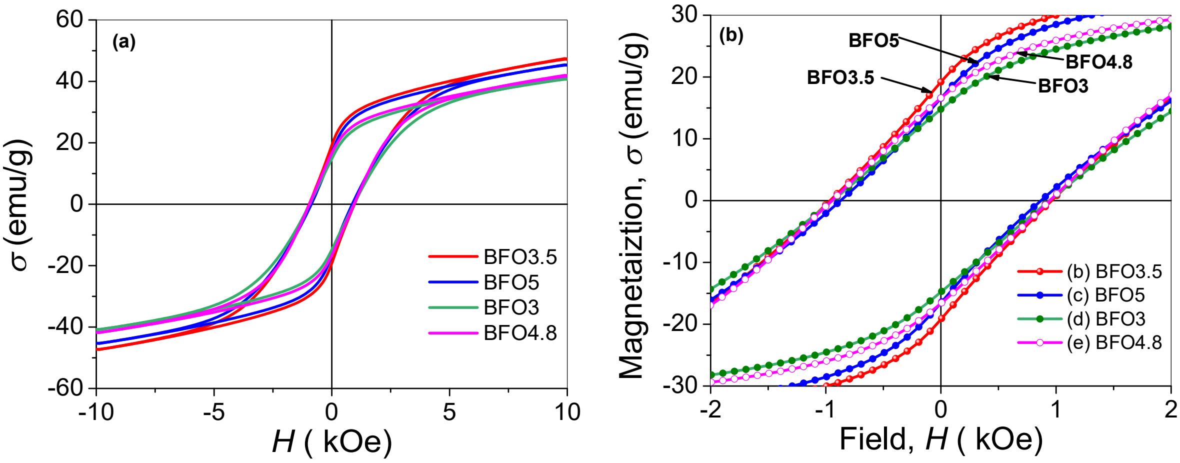

FIG. 7. (a) hysteresis loops and (b) expanded view of the hysteresis loops for the samples.

TABLE 4. Saturation magnetization (σ_s), remanence (σ_r), squareness ratio (σ_r/σ_s), coercive field (H_c), and anisotropy field (H_a) for the samples.

Sample	σ_s (emu/g)	σ_r (emu/g)	σ_r/σ_s	H_c (Oe)	H_a (kOe)
BFO3	45.1	14.8	0.33	947	12.1
BFO3.5	52.1	19.0	0.36	966	11.8
BFO4.8	46.2	16.6	0.35	947	12.1
BFO5	49.9	16.6	0.33	878	11.7

Other magnetic parameters such as the saturation magnetization (σ_S) and magnetocrystalline anisotropy field (H_a) were obtained from the law of approach to saturation. At high fields, the magnetization behavior is determined by the rotation of the domain magnetization into the direction of the applied field and the magnetization can be approximated by the polynomial [42, 43]:

$$M = M_s\left(1 - \frac{A}{H} - \frac{B}{H^2}\right) + \chi H \qquad (4)$$

Here, $M_s = \rho_x \sigma_s$ is the saturation magnetization per unit volume, the constant A represents the contribution of crystal imperfections and the constant B represents the contribution of the magnetocrystalline anisotropy ($B = H_a^2/15$). At high fields, the contributions of the crystal imperfections and the forced magnetization term, χH, are negligible, leading to a linear relation between M and $1/H^2$, which can also be expressed as a linear relation between σ and $1/H^2$ as follows:

$$\sigma = \sigma_s\left(1 - \frac{B}{H^2}\right) \qquad (5)$$

Note that this simple equation which involves the directly measured magnetization $\sigma(H)$ is obtained by canceling the density on the two sides of the equation. The straight line fit to the experimental data in the field range 8.5 kOe $\leq H \leq$ 10 kOe allowed determination of the best estimate of the saturation magnetization (σ_s = the intercept of the line with the magnetization axis) and the magnetocrystalline anisotropy (from the slope of the straight line) and the results are listed in Table 4. The saturation magnetization of the samples (45.1 to 52.1 emu/g) were in agreement with reported values of 49 and 51 emu/g [35, 44], but lower than the best values of 70 – 72 emu/g obtained by our group [38, 45, 46]. The squareness ratio (σ_r/σ_s) for all samples was in the range of 0.33 – 0.36, appreciably lower than the value characteristic of randomly oriented single-domain particles of 0.5, which confirms the multi-domain nature of a significant fraction of the particles in our samples. Among these samples, the highest and best magnetic parameters for high-density magnetic recording were exhibited by the sample BFO3.5, with σ_s = 52.1 emu/g, σ_r = 19.0 emu/g and H_c = 966 Oe.

The magnetocrystalline anisotropy field (H_a) was almost the same (11.9 ± 0.2 kOe) for all samples. These values are in good agreement with values reported for a variety of BaM hexaferrites exhibiting high coercivity (> 4 kOe) [47]. This indicates that the observed reduction of the coercivity of the samples in this study is not caused by lowering the magnetocrystalline anisotropy, which is a further confirmation that this reduction is associated with particle size [48].

Thermomagnetic Measurements

Fig. 8 shows the thermomagnetic curves for the samples at a constant applied field of 100 Oe. The curves exhibited normal slow decrease of the magnetization with the increase of temperature and then a sudden drop associated with ferrimagnetic to paramagnetic phase transition at the Curie temperature. The Curie temperature (indicated by the arrow in Fig. 8) of all samples was (455 ± 5) °C, characteristic of barium M-type hexaferrite [34]. All curves, with the exception of that for the sample BFO5, exhibited a normal behavior characteristic of a single magnetic phase. Notice that α-Fe_2O_3 undergoes a transition from antiferromagnetic to paramagnetic state above Neel temperature (T_N ~ 687 °C) and thus does not exhibit magnetic phase transition in the temperature range adopted in this study. The curve of the sample BFO5, however, exhibited a small peak just below the Curie temperature (Hopkinson peak), indicating the presence of a small fraction of superparamagnetic particles [49]. Also, the curve is flattened above the Curie temperature, indicating the possibility of existence of magnetic inhomogeneity in this sample.

Conclusion

We have demonstrated that iron-rich powders extracted from solid wastes such as scrap iron filings can profitably replace other costly iron sources in the production of important magnetic oxides. The results of this study clearly indicated that powders obtained by firing iron filings at 500 °C provide a useful metallic iron source, whereas the powder obtained by sintering at 1200 °C can be reliably used as an iron oxide source. Both sources were successfully used in this study for the production of high-quality BaM hexaferrites. The magnetic parameters of the prepared hexaferrites were characteristic of materials suitable for high-density magnetic storage media and permanent magnets for applications that do not require high-flux and magnetically hard materials. The procedure adopted in this study can be modified and extended to other metal scrap for the production of important materials, thus reducing the level of hazardous solid waste and lowering the cost of production.

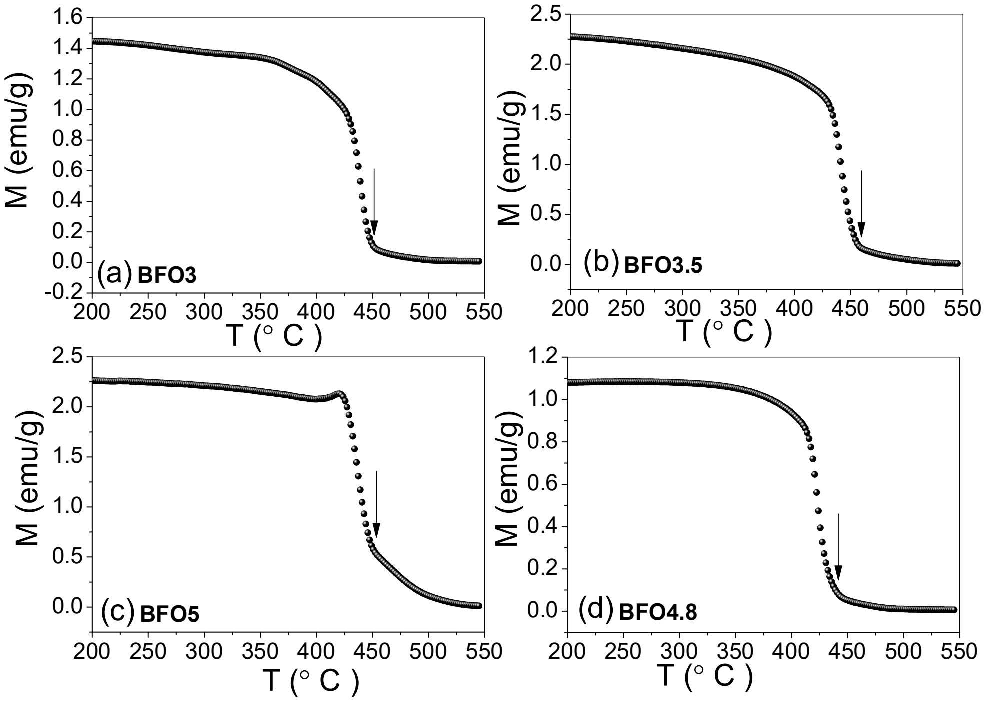

FIG.8. Thermomagnetic curves (at an applied field of 100 Oe) for the samples.

Acknowledgement

S.H. Mahmood would like to acknowledge the support provided by the University of Jordan during his sabbatical leave at Michigan State University. The technical assistance of Y. Abu Salha (the University of Jordan) in performing XRD measurements is acknowledged. Also, the assistance of Zaid Al-Degess (the mechanical workshop at the Physics Department, the University of Jordan) in collecting iron filings for this study is acknowledged.

References

[1] Ohimain, E.I., Journal of Environmental Management and Public Safety, 2 (2013) 1.

[2] Carvalheiras, J., Novais, R.M., Mohseni, F., Amaral, J.S., Seabra, M.P., Labrincha, J.A. and Pullar, R.C., Ceramics International, 46 (2020) 5757.

[3] Liu, Z. and Li, H., Hydrometallurgy, 155 (2015) 29.

[4] Khairul, M.A., Zanganeh, J. and Moghtaderi, B., Conservation & Recycling, 141 (2019) 483.

[5] Özgür, Ü., Alivov, Y. and Morkoç, H., Journal of Materials Science: Materials in Electronics, 20 (2009) 789.

[6] Pullar, R.C., Progress in Materials Science, 57 (2012) 1191.

[7] Harris, V.G., Geiler, A., Chen, Y., Yoon, S.D., Wu, M., Yang, A., Chen, Z., He, P., Parimi, P.V. and Zuo, X., Journal of Magnetism and Magnetic Materials, 321 (2009) 2035.

[8] Mahmood, S.H., "Permanent Magnet Applications", In: S.H. Mahmood and I. Abu-Aljarayesh (Eds.), "Hexaferrite Permanent Magnetic Materials", (Materials Research Forum LLC, Millersville, PA, 2016), pp. 153-165.

[9] Gutfleisch, O., Willard, M.A., Brück, E., Chen, C.H., Sankar, S. and Liu, J.P., Advanced Materials, 23 (2011) 821.

[10] Strnat, K.J., Proceedings of the IEEE, 78 (1990) 923.

[11] Meng, P., Xiong, K., Wang, L., Li, S., Cheng, Y. and Xu, G., Journal of Alloys and Compounds, 628 (2015) 75.

[12] Lee, J., Hong, Y.-K., Lee, W., Abo, G.S., Park, J., Neveu, N., Seong, W.-M., Park, S.-H. and Ahn, W.-K., Journal of Applied Physics, 111 (2012) 07A520.

[13] Cui, J., Kramer, M., Zhou, L., Liu, F., Gabay, A., Hadjipanayis, G., Balasubramanian, B. and Sellmyer, D., Acta Materialia, 158 (2018) 118.

[14] Sugimoto, S., Okayama, K., Kondo, S.-I., Ota, H., Kimura, M., Yoshida, Y., Nakamura, H., Book, D., Kagotani, T. and Homma, M., Materials Transactions, JIM, 39 (1998) 1080.

[15] Chikazumi, S., "Physics of Ferromagnetism", 2nd edn., (Oxford University Press Oxford, 2009).

[16] Mahmood, S.H., Aloqaily, A.N., Maswadeh, Y., Awadallah, A.M., Bsoul, I., Awawdeh, M. and Juwhari, H.K., Solid State Phenomena, 232 (2015) 65.

[17] Mahmood, S.H., Zaqsaw, M.D., Mohsen, O.E., Awadallah, A.M., Bsoul, I., Awawdeh, M. and Mohaidat, Q.I., Solid State Phenomena, 241 (2016) 93.

[18] Albanese, G., Le Journal de Physique Colloques, 38 (1977) 85.

[19] Mahmood, S.H., "High-performance Permanent Magnets", In: S.H. Mahmood and I. Abu-Aljarayesh (Eds.), "Hexaferrite Permanent Magnetic Materials", (Materials Research Forum LLC, Millersville, PA, 2016), pp. 47-73.

[20] Mahmood, S.H. and Bsoul, I., "Tuning the magnetic properties of M-type hexaferrites", In: R.B. Jotania and S.H. Mahmood (Eds.), "Magnetic Oxides and Composites", (Materials Research Forum LLC, Millersville, PA, USA, 2018), pp. 49-100.

[21] Mahmood, S.H., "Ferrites with High Magnetic Parameters", In: S.H. Mahmood and I. Abu-Aljarayesh (Eds.), "Hexaferrite Permanent Magnetic Materials", (Materials Research Forum LLC, Millersville, PA, 2016), pp. 111-152.

[22] Rietveld, H.M., Journal of Applied Crystallography, 2 (1969) 65.

[23] Rodriguez-Carvajal, J., IUCR Newsletter, 26 (2001) 12.

[24] Roisnel, T. and Rodrigez-Carvajal, J., "A Windows Tool for Powder Diffraction Patterns Analysis", In: R. Delhez and E.J. Mittemeijer (Eds.), "The Seventh European Powder Diffraction Conference (EPDIC 7)", (Trans Tech Publications, Barcelona, Spain, 2000), pp. 118-123.

[25] Mahmood, S.H., Awadallah, A.M., Maswadeh, Y. and Bsoul, I., IOP Conference Series: Materials Science and Engineering, 92 (2015) 012008.

[26] Ahmadzadeh, M., Romero, C. and McCloy, J., AIP Advances, 8 (2018) 056807.

[27] Tadic, M., Panjanb, M., Damnjanovic, V. and Milosevic, I., Applied Surface Science, 320 (2014) 183.

[28] Mahmood, S.H., Ghanem, A.A., Bsoul, I., Awadallah, A. and Maswadeh, Y., Materials Research Express, 4 (2017) 036105.

[29] Maswadeh, Y., Mahmood, S.H., Awadallah, A.M. and Aloqaily, A.N., IOP Conference Series: Materials Science and Engineering, 92 (2015) 012019.

[30] Shin, S.S. and Kwon, S.-J., Powder Diffraction, 7 (1992) 212.

[31] Stergiou, A.C., Samaras, D., Kalogirou, O., Vincent, H. and Bekka, A., Solid State Ionics, 50 (1992) 11.

[32] Awadallah, A.M., Mahmood, S.H., Maswadeh, Y., Bsoul, I. and Aloqaily, A.N., IOP Conference Series: Materials Science and Engineering, 92 (2015) 012006.

[33] Albanese, G. and Deriu, A., Ceramics International, 5 (1979) 3.

[34] Smit, J. and Wijn, H.P.J., "Ferrites", (Wiley, New York, 1959).

[35] Soman, V.V., Nanoti, V.M. and Kulkarni, D.K., Ceramics International, 39 (2013) 5713.

[36] Warren, B.E., "X-ray Diffraction", (Addison-Wesley, Reading, Massachsetts, 1969).

[37] An, S.Y., Shim, I.-B. and Kim, C.S., Journal of Applied Physics, 91 (2002) 8465.

[38] Bsoul, I. and Mahmood, S., Jordan J. Phys., 2 (2009) 171.

[39] Shepherd, P., Mallick, K.K. and Green, R.J., Journal of Magnetism and Magnetic Materials, 311 (2007) 683.

[40] Rezlescu, L., Rezlescu, E., Popa, P. and Rezlescu, N., Journal of Magnetism and Magnetic Materials, 193 (1999) 288.

[41] Abu-Aljarayesh, I., "Magnetic Recording", In: S.H. Mahmood and I. Abu-Aljarayesh (Eds.), "Hexaferrite Permanent Magnetic Materials", (Materials Research Forum LLC, Millersville, PA, 2016), pp. 166-181.

[42] Cullity, B.D. and Graham, C.D., "Introduction to Magnetic Materials, 2nd edn., (John Wiley & Sons, Hoboken, NJ, 2011).

[43] Grössinger, R., Physica Status Solidi (a), 66 (1981) 665.

[44] Topal, U., Materials Science and Engineering: B, 176 (2011) 1531.

[45] Mahmood, S.H., Aloqaily, A.N., Maswadeh, Y., Awadallah, A., Bsoul, I. and Juwhari, H., Material Science Research India, 11 (2014) 09.

[46] Bsoul, I. and Mahmood, S., Journal of Alloys and Compounds, 489 (2010) 110.

[47] Awawdeh, M., Bsoul, I. and Mahmood, S.H., Journal of Alloys and Compounds, 585 (2014) 465.

[48] Sharma, P., Roch, R.A., Medeiros, S.N., Hallouche, B. and Paesano Jr, A., Journal of Magnetism and Magnetic Materials, 316 (2007) 29.

[49] Mahmood, S.H. and Bsoul, I., EPJ Web of Conferences, 29 (2012) 00039.